Smart Structures and Systems, *Vol. 18, No. 1 (2016) 93-115*
DOI: http://dx.doi.org/10.12989/sss.2016.18.1.093

An experimental study of vibration control of wind-excited high-rise buildings using particle tuned mass dampers

Zheng Lu*[1], Dianchao Wang[1], Sami F. Masri[2] and Xilin Lu[1]

[1]*State Key Laboratory of Disaster Reduction in Civil Engineering, Tongji University, No. 1239, Siping Road, Shanghai, China*
[2]*Viterbi School of Engineering, University of Southern California, Los Angeles, California 90089, USA*

(Received September 26, 2015, Revised April 21, 2016, Accepted May 6, 2016)

Abstract. A particle tuned mass damper (PTMD) system is the combination of a traditional tuned mass damper (TMD) and a particle damper (PD). This paper presents the results of an experimental and analytical study of the damping performance of a PTMD attached to the top of a benchmark model under wind load excitation. The length ratio of the test model is 1:200. The vibration reduction laws of the system were explored by changing some system parameters (including the particle material, total auxiliary mass ratio, the mass ratio between container and particles, the suspending length, and wind velocity). An appropriate analytical solution based on the concept of an equivalent single-unit impact damper is presented. Comparison between the experimental and analytical results shows that, with the proper use of the equivalent method, reasonably accurate estimates of the dynamic response of a primary system under wind load excitation can be obtained. The experimental and simulation results show the robustness of the new damper and indicate that the damping performance can be improved by controlling the particle density, increasing the amount of particles, and aggravating the impact of particles etc.

Keywords: particle tuned mass damper system; wind tunnel experiment; vibration control; simulation; impact dampers

1. Introduction

During the past decades, high-rise buildings have developed prosperously with the increasing application of high-strength and lightweight materials, and have brought much convenience to people's life. However, these high-rise buildings, especially the super-tall buildings, are much more likely to suffer wind load which tend to be a control factor in the design process. In general, the vibration response of across-wind direction is larger than that of along-wind direction, for buildings higher than 300 m (Gu and Quan 2004), and the excessive displacement and acceleration at the top of the building will cause discomfort feelings in the occupants. Moreover, the aeroelastic instability of high-rise building under wind load is very common, which will exaggerate the vibration of super-tall buildings (Piccardo *et al.* 2015, Dell'Isola *et al.* 2015). Therefore, it is essential to take some measures to control the excessive vibration response under wind excitation.

Since Yao (1972) introduced the concept of vibration control to civil engineering in 1972, the

*Corresponding author, Associate Professor, E-mail: luzheng111@tongji.edu.cn

http://www.techno-press.org/?journal=sss&subpage=8 ISSN: 1738-1584 (Print), 1738-1991 (Online)

relevant theory and methods have developed significantly. Scholars from all over the world have proposed various control strategies (Housner *et al*. 1997), which can be classified as active control (Gu and Peng 2002, Sharma *et al.* 2015), passive control (Chen and Lu 2008, Aly 2014,Warnitchai and Hoang 2006), hybrid control (Philips *et al.* 2014), and semi-active control (Esteki *et al.* 2015). Passive control is a prevalent strategy due to its independence from reliance on extra energy input. Among numerous passive control devices, the TMD is most widely used in wind-induced vibration control due to its simple characteristics, convenient installation, low cost, and favorable control effects under specific tuned frequencies (Aly 2013). Many tall buildings were constructed with a TMD, such as Shanghai Tower in Shanghai (Lu and Chen 2011 a,b), Taipei 101 in Taipei, John Hancock building in Boston (Campbell 1995), Citicorp Center Office Building in New York (Petersen 1980), Chiba Port Tower in Japan and the Miliad Tower in Iran (Ghorbani *et al*. 2009). Many aero-elastic wind tunnel experiments of various tall building models with tuned mass dampers were also conducted.

Vickery *et al*. (1970) conducted an aero-elastic model test of a proposed structure with tuned mass dampers and carried out parametric studies based on a two-degree-of-freedom system model and white noise excitation. Tanaka and Mark (1983) conducted a parametric study of the tuned mass damper based on the aero-elastic wind tunnel test of a 1:1000 scaled model of the CAARC Standard Tall Building. If properly tuned, a TMD can effectively suppress excessive vibrations. However, the very narrow band of suppression frequency, ineffective reduction of non-stationary vibrations, and sensitivity problems due to mistuning, are the inherent limitations of a conventional TMD. According to field measurements and analysis of two buildings in the Caltech campus by John F. Clinton *et al.* (2006), their natural vibration frequency varies with the changing of surrounding environment, such as wind velocity, temperature, relative humidity, and the type of earthquakes, as well as the changing of the building's function. Consequently, it is essential to propose a passive control device with a better robustness of damping performance under a wide band of frequencies.

Particle damping technology is also a passive control technology, which dissipates the vibration energy by collisions and friction between particles, or between particles and their container (Bryce *et al*. 2000, Lu *et al.* 2010). The particles are made of metallic or non-metallic materials, and they are placed in a space-limited container. The advantages of slight change to the primary structure, a wide reduction frequency band, and insensitivity to environmental changes make the particle damper preferable to traditional passive control devices. It has been widely researched and applied in machinery and aviation engineering, and the damping performance is favorable (Sims *et al*. 2005, Hu *et al.* 2008), but the research in civil engineering is just in the early stages and is only limited in the area of earthquake-induced vibration control.

Some experimental studies and numerical simulations have been carried out for the characterization of the particle damper. Papalou verified the test results of the particle damper by equating the multi-unit particle damper to a single particle impact damper based on certain equivalent principles (Papalou and Masri 1996), and investigated the effectiveness of the particle damper in reducing the vibrations of multi-drum ancient columns experimentally (Papalou and Strepelias 2014). Lu *et al.* (2012) conducted a shaking table test of a three-story steel frame with a particle damper, and evaluated the effects of a large number of system parameters (such as number, size and material of the particles, mass ratio, excitation frequency, coefficient of restitution, and the coefficient of friction) based on the discrete-element method (Lu *et al*. 2011a,b). Yan *et al.* (2013) carried out a series of shaking table tests of a 1/10-sacle model bridge with and without tuned particle dampers to evaluate the performance of the system, and put forward a finite element

method for numerical simulation based on energy considerations. Naeim *et al.* (2011) introduced the performance of a tall building with a particle damper system in Santiago, Chile during the 2010 offshore Maule, Chile earthquake, suggesting that the system performed very well during the earthquake, and that the building did not suffer any damage above the ground, or at any subterranean floors and basement walls. The above results show that the damping performance of the particle damper is robust under earthquake excitations (Lu *et al*. 2014).

As to the simulation of impact behaviors in particle damper problem, considering its physical natural, such impact phenomenon can usually be modeled in two different models: the soft-impact model (model the contact as a linear or Herzian spring, which lead to separate motion equations for out- and for in-of-contact cases) and the hard-impact model (impact oscillators, assuming an instantaneous contact with a coefficient of restitution) (Chiaia *et al.* 2015). The research of Andreaus *et al.* (2010, 2013a, b, 2016) showed that the prescription of velocity after impact between deformable bodies has an intrinsic indeterminacy (hyperstaticity of hard-impact dynamics) of impacts between deformable bodies, this can be overcome by the use of soft impact dynamics.

Despite all these efforts, numerous questions remain to be answered to understand the physics of the complex nonlinear performance of particle dampers, especially under wind load. In this paper, a particle tuned mass damping system is proposed, by combining the particle damper technology and the tuned mass damper technology. The combined damper can dissipate the input energy not only by tuning the frequency just like the traditional TMD, but also by collisions, impacts, and friction between particles, or between particles and the container wall. An aero-elastic wind tunnel experiment was designed by attaching the PTMD to a 1/200-scale benchmark model, and conducted in the TJ-2 boundary layer wind tunnel in the State Key Laboratory of Disaster Reduction in Civil Engineering, Tongji University. The PTMD is a simple pendulum with a wooden container being attached to four identical round lines, which was secured to the top cover of the building model, and the container can swing freely at the top space. The natural frequency of the damper can be adjusted by changing the suspending length of the supporting round lines. The influence of the following parameters was investigated: particle material, total auxiliary mass ratio, mass ratio of the container to particles, suspending length, and wind velocity. The results show that different parameters have different influence on the damping performance, and that the influence law is consistent with that observed under seismic excitation.

An approximate analytical solution, based on the generalization of the experimental results using the concept of an equivalent single-unit impact damper, is presented for estimating the primary system response levels when operating in the vicinity of the optimum combination of system parameters. The analytical results match the experimental results of the building model with the dampers very well.

2. Experimental set-up

2.1 Model design

The Benchmark model which was used for the response control of wind-excited tall buildings was chosen to represent a typical high-rise building. The prototype of the benchmark model is a 76-story 306 meters concrete office tower proposed for the city of Melbourne, Australia. The building is slender with a height to width ratio of 7.3; hence, it is wind sensitive. The benchmark

building is symmetric in both horizontal directions, and the axis of elastic center coincides with the axis of mass center (Samali *et al*. 1999, Yang *et al*. 2004). The length scale ratio is 1:200 according to the maximum blocking ratio of the wind tunnel experiment, and the other similitude ratios are calculated from the length ratio, based on the pneumatic similarity requirement (ASCE, 2003), listed in Table 1. The shape and first mode of the building have great effects on the wind-excited response; consequently, it is very important to simulate them properly. In this experiment, the model was mainly composed of a core steel beam, additional mass, and outwear. The steel beam and the additional mass were used to ensure that the first mode and frequency of the model building was the same as that of the prototype building, and the outwear was used to simulate the shape of the prototype building.

The cross-sectional shape of the steel beam is square and its size is 15 mm×15 mm, which was welded on the baseboard. The material of the attached mass is lead, for its high density, and the total mass of the attached mass, steel beam and outwear is 19.2 Kg. The organic glass with 2 mm thickness was chosen as the outwear material, and 2 mm seams were set up at regular intervals along the height direction. The model was equally separated into three parts at the height direction. Two acceleration sensors, together with two displacement sensors, were set up in pairs at the top of each part, in order to measure the acceleration and displacement time histories of the model at different heights. The schematic drawings of the benchmark model and the location of the sensors are shown in Fig. 1.

2.2 Wind environment design

The TJ-2 wind tunnel at Tongji University is a boundary layer tunnel of the closed-circuit type. The working section of the tunnel is 3 m wide, 2.5 m high and 15 m long. The achievable mean wind speed ranges from 0.5 m/s to 68.0 m/s, adjustable continuously. The simulation of the atmospheric boundary layer is through the arrangement of a series of roughness elements and joists from the upstream of the wind flow. The test wind velocities are determined according to the design wind pressures of several main cities in China, which are specified in the *Load Code for the Design of Building Structures (GB 5009-2012)*. The corresponding relations are listed in Table 2.

According to the Chinese code, the wind profile based on exponential expressions, are shown in Eq. (1)

$$\frac{\bar{v}(\mathrm{z})}{\bar{v}(\mathrm{b})}=\left(\frac{z}{z_b}\right)^{\alpha} \tag{1}$$

where z_b and $\bar{v}(\mathrm{b})$ are the standard height and average wind velocity, respectively; z and $\bar{v}(\mathrm{z})$ are the height at any point and corresponding average wind velocity, respectively; α is the ground roughness exponent, whose value is 0.22 in the C-type wind field specified in the *Load Code for the Design of Building Structures* (*GB 5009-2012)*, in which most of the high-rise buildings are located. The simulations of the wind velocity, turbulence profile, and wind power spectrum of the C category at height of 150cm in wind tunnel are shown in Fig. 2. The test data in those three figures match fairly well with the theoretical values which are regulated in the *Load Code for the Design of Building Structures* (*GB 5009-2012)*. Therefore, it can be concluded that the wind environment simulation in TJ-2 wind tunnel is quite accurate.

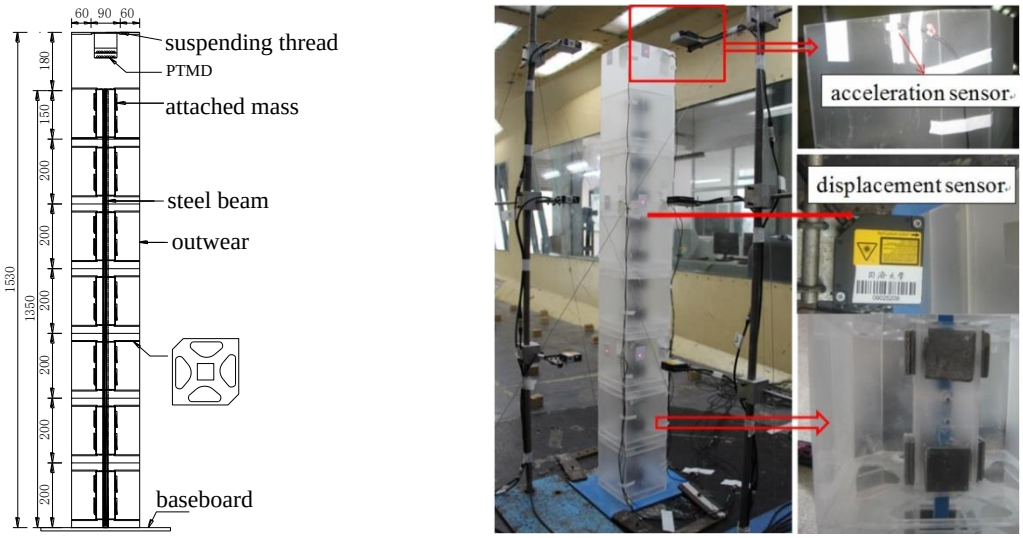

(a) Experimental model (b) Sensors arrangement

Fig. 1 Experiment setup

Table 1 Main similarity parameters of the model

Parameters	Similitude ratio	Similitude requirement	Parameters	Similitude ratio	Similitude requirement
Length	$\lambda_L = 1:200$	Geometric similarity ratio	Displacement	$\lambda_d = \lambda_L = 1/200$	Dimension
Frequency	$\lambda_f = \lambda_v / \lambda_L = \sqrt{200}:1$	Strouhal	Acceleration	$\lambda_a = \lambda_L \lambda_f^2 = 1$	Dimension
Time	$\lambda_t = 1:\lambda_f = 1:\sqrt{200}$	Strouhal	Gravitational Acceleration	$\lambda_g = 1$	Unchanged
Velocity	$\lambda_v = 1/\sqrt{\lambda_L} = 1/\sqrt{200}$	Froude	Density	$\lambda_\rho = 1$	Unchanged

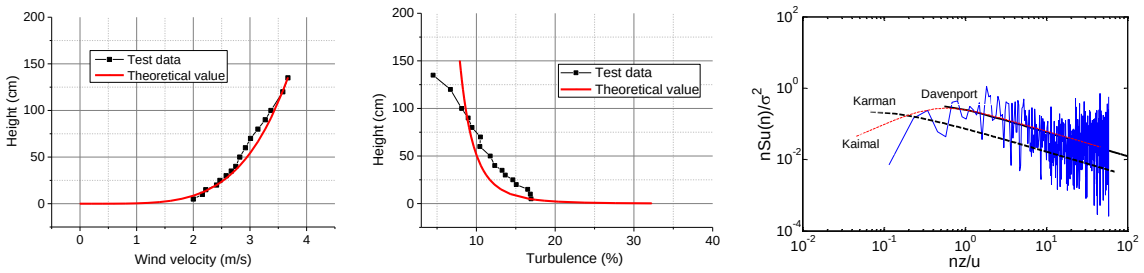

(a) Wind velocity profile (b) Turbulence profile (c) Wind power spectra of C category at height of 150 cm

Fig. 2 Wind environment simulation

Table 2 Actual wind pressure and corresponding wind velocity in wind tunnel

Reference wind pressure (kN/m^2)	0.50	0.65	0.80	1.0
Wind velocity in wind tunnel(m/s)	3.5	4.0	4.5	5.0

(a) First layer with copper particles

(b) Second layer with copper particles

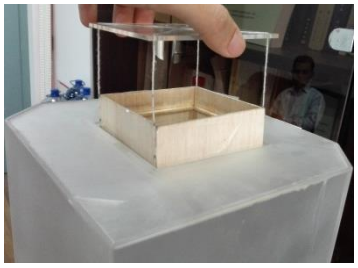

(c) Suspending location at the top of the model

Fig. 3 PTMD configuration

2.3 PTMD design

In the experiment, the particle damper was suspended by four nylon cords with the same length from the top of the model (as shown in Fig. 3(c)), and the tuning frequency can be changed by adjusting the suspending length. The square container was made by firmly splicing together lightweight wooden plates (as shown in Fig. 3). Four different materials (steel, copper, lead and tungsten carbide) were chosen, in which the diameter of lead particles ranged from 2 mm~10 mm and the other three were 6 mm.

Finally, the total mass of the model is 19.2 Kg; the mass of the container is 10 g; the mass ratio of the container to particles is 0.056 when the total auxiliary mass ratio of damper to model is 1%. Since some experimental cases may need large number of particles, to avoid being piled up, such particles are distributed into several identical layers, shown in Figs. 3(a) and 3(b).

3. Dynamic characteristics of the model

To obtain the dynamic characteristics of the test model, free vibration experiments were conducted by applying an initial displacement at the top of the model, in different directions. The model vibrated in the across-wind direction when the initial displacement was exerted in the along-wind direction (as shown in Fig. 4(a)), indicating that the vibrations of the two directions were coupling together. This is because of the close frequency of the primary structure in both directions, thus causing resonance. Based on the centro-symmetric design of the structure, the stiffness, frequency, and damping ratio in the two directions can be assumed to be the same; hence, the damping ratio can be calculated by the relevant formula used in structural dynamics (Quan 2002), and the combined displacement (using SRSS (square root of sum square) method, sqrt (x^2+y^2)) time history of the two directions is shown in Fig. 4(b). The calculated characteristics of the model are listed in Table 3.

Table 3 Dynamic characteristics of the model

	Along-wind	Across-wind
Natural frequency (Hz)	2.16	2.17
Damping ratio	0.3%	0.3%

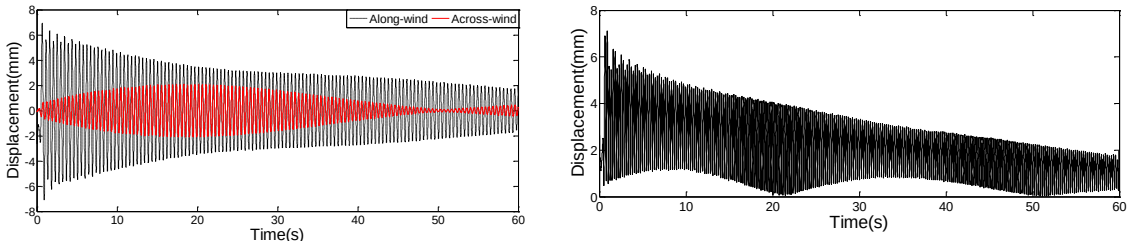

(a) Time history curve in both directions (b) Combined displacement time history curve

Fig. 4 Model displacement response under free vibration with an initial displacement in the along-wind direction

4. Parameter analysis

The acceleration peak value and inter-story drift are important controlling indexes in the design process of high-rise buildings which are regulated in the Chinese code, and too large acceleration values may cause discomfort feelings in the occupants. The root-mean-square (RMS) is an indicator of the vibration energy, and the whole time history of the acceleration and displacement are essential in evaluating the structural damage. Therefore, the peak value and the RMS value of the acceleration and displacement are chosen to evaluate the damping performance of the PTMD. The vibration reduction effect is defined as follows:

$$\frac{\text{(peak response of uncontrolled model) - (peak response of controlled model)}}{\text{(peak response of uncontrolled model)}} \times 100\%$$

The focus of this paper is on the performance of the PTMD attached to a high-rise building model under wind load. Consequently, the influence of the following system parameters is investigated: particle density, total auxiliary mass ratio, mass ratio of the container to particles, suspending length, and wind velocity.

4.1 Effects of particle density

The influence of particle density on the damping performance of the PTMD was examined by using four different materials: tungsten carbide, lead, steel and copper. The total auxiliary mass ratio (1%), the diameter (6 mm for all the particles), the container size (8.5 cm×8.5 cm, 1 layer) and the wind velocity (4 m/s) were kept constant.

Fig. 5 shows that the vibration reduction effects of the RMS and the peak value response are

favorable in both across-wind and along-wind directions. For the across-wind response, the effects improve with the particle density decreasing. This is due to the fact that the decrease of the particle density leads to the increase of particle number, and consequently results in the increase of energy consumption through particle collisions and friction. In fact, the density of the tungsten carbide is twice the density of steel; consequently, for the same mass, the number of steel particles is twice the number of the tungsten carbide ones. In this experiment, the occupying area of the steel particles is around 80% of the container, with no particle piling up. The particles can move freely and energetically, leading to high momentum exchange and energy dissipation.

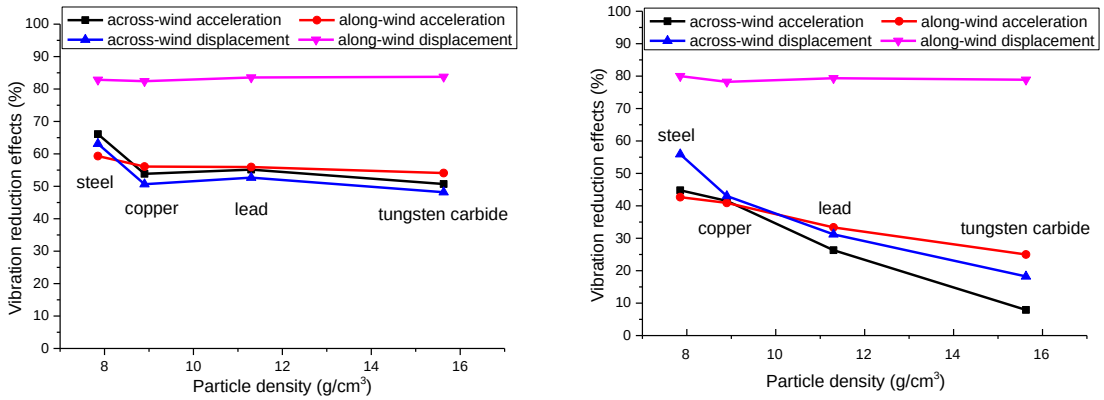

(a) RMS reduction effects (b) Peak value reduction effects

Fig. 5 Vibration reduction effects under different particle densities

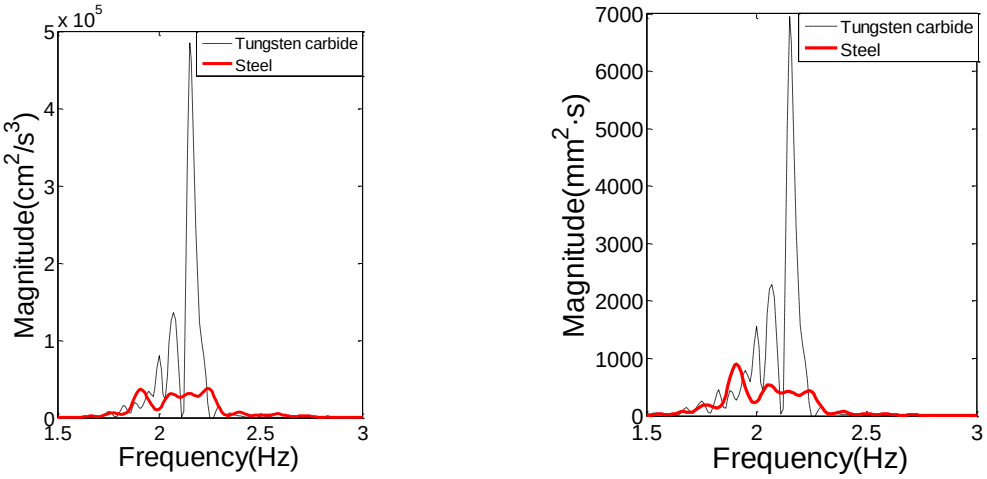

(a) Acceleration response (b) Displacement response

Fig. 6 Power spectral density under tungsten carbide and steel particles

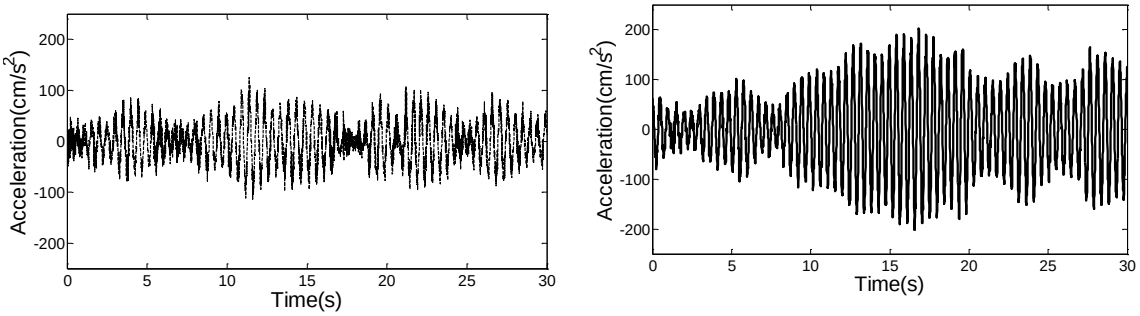

(a) Controlled structure (steel particle case) (b) Uncontrolled structure

Fig. 7 The across-wind acceleration time history under different conditions

When comparing Fig. 5(a) with Fig. 5(b), it is not hard to find that the vibration reduction effects of the peak response are much more sensitive to the effects of particle density, that is, the vibration reduction effects drops significantly when the particle density increases. Furthermore, as can be seen from the corresponding power spectrum in Fig. 6, the vibration energy mainly concentrates in the fundamental frequency under the tungsten carbide condition, while the frequency band is broader, and the peak value of magnitude is much smaller, under the steel condition. The above analyses and conclusions show that it is a good strategy to improve the damping performance by minimizing the particle density under reasonable condition (i.e., the total mass stays the same and particles do not pile up), thus the vibration response of the primary structure can be effectively reduced by transferring more vibration energy to the attached PTMD. More importantly, the vibration energy of the primary structure can be distributed over a wider frequency band with the particle density decreasing.

On the other hand, the typical comparative dynamic responses of the controlled structure and uncontrolled structure are shown in Figs. 7 and 8. As can be seen from the time history curves in Fig. 7, the magnitude of the controlled structure is much smaller than that of the uncontrolled one, and the acceleration response is significantly reduced for the whole time history. Similarly, as shown in Fig. 8, the magnitude and the whole response of the displacement of the controlled structure are effectively suppressed. These figures clearly show that the incorporated PTMD can effectively control the structure's vibration.

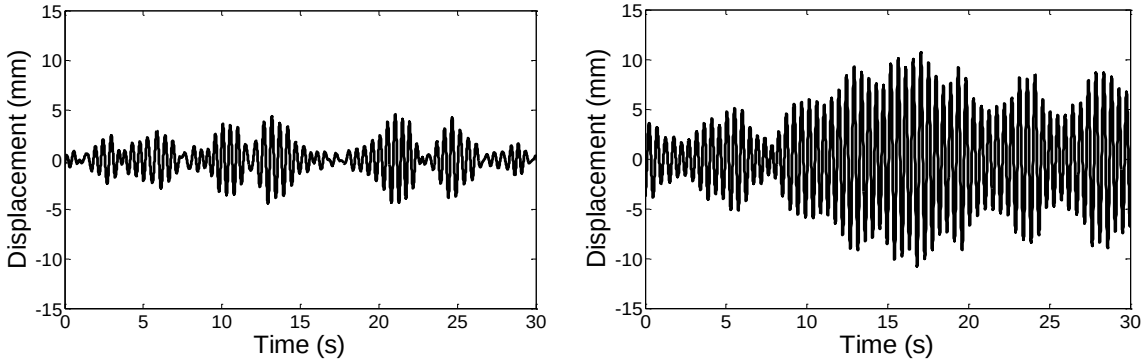

(a) Controlled structure (steel particle case) (b) Uncontrolled structure

Fig. 8 The across-wind displacement time history under different conditions

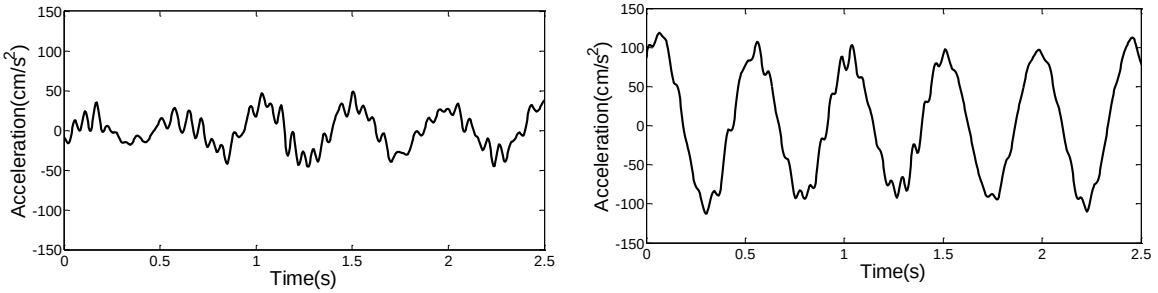

(a) Controlled structure (steel particle case) (b) Uncontrolled structure

Fig. 9 The across-wind acceleration time history under different conditions

The high resolution plot for 5 periods of the controlled and uncontrolled acceleration time history curves are shown in Fig. 9, in which small high-frequency components are distributed evenly along the whole curve in Fig. 9(a), while the curve in Fig. 9(b) is much smoother than that in Fig. 9(a). This is because the vibration of the PTMD leads to violent collisions between particles or between the particles and the container wall. The high frequency collisions will stimulate the high-order frequency vibration of the main structure, and the corresponding character in the acceleration time history curve is the appearance of the evenly distributed high-frequency components. Moreover, the magnitude of these components is not too large, as would have been the case of a single-particle impact damper. This is due to the impact forces produced by the collisions between the small particles are not too large to change the movement of the structure impulsively. The reduction effects of the PTMD under wind load excitation are robust and more stable than the traditional impact damper.

4.2 Effects of total auxiliary mass ratio

The effects of total auxiliary mass ratio were examined by employing different mass ratios: 0.5%, 0.75%, 1% and 1.25%. The particle material (steel), the diameter (6 mm) for all the particles, the container size (8.5 cm×8.5 cm, 2 layers) and the wind velocity (4 m/s) were kept constant.

The vibration reduction effects under various mass ratios are presented in Fig. 10. Higher values of the mass ratio result in a reduction of response, but the reduction is not linearly proportional to the increase of the mass ratio, and when the mass ratio is 1.25, the reduction effect is sometimes lower than the condition of the mass ratio equal to 1. The reason for this phenomenon is that a higher mass ratio means larger amount of particles, resulting in more vibration energy consumed by collision and friction between particles. But too many particles may pile up, and this will decrease the effectiveness of momentum exchange, thus giving rise to the nonlinearity between damping effects and mass ratios.

Another interesting observation that can be gleaned from Fig. 10 is that indefinitely increasing the mass of the particles may not reduce the response any further. This phenomenon can be explained by considering the conservation of momentum between the particles and the system. As a specific particle's mass increases, its velocity immediately after the impact decreases. The force of friction also contributes to the reduction in the velocity while the particle is in motion. As the mass increases beyond a certain value, its velocity immediately after the impact does not allow it

to overcome the frictional force, and it comes to rest relative to the system prior to getting the next collision with the container. It is possible for the particle to oscillate within the container's boundaries (without touching the walls), while the system goes through several cycles of motion before making the next impact.

From the corresponding power spectrum shown in Fig. 11, the vibration energy of the primary structure is distributed almost in the same frequency band, but the peak value of the magnitude is not at the same level. The peak value of both the acceleration and displacement power spectral density in the case of 1% are smaller than that in the case of 0.5%. This indicates that increasing the mass ratio transfers more vibration energy to the attached PTMD and, at the same time, the frequency band distribution of vibration energy is not changed.

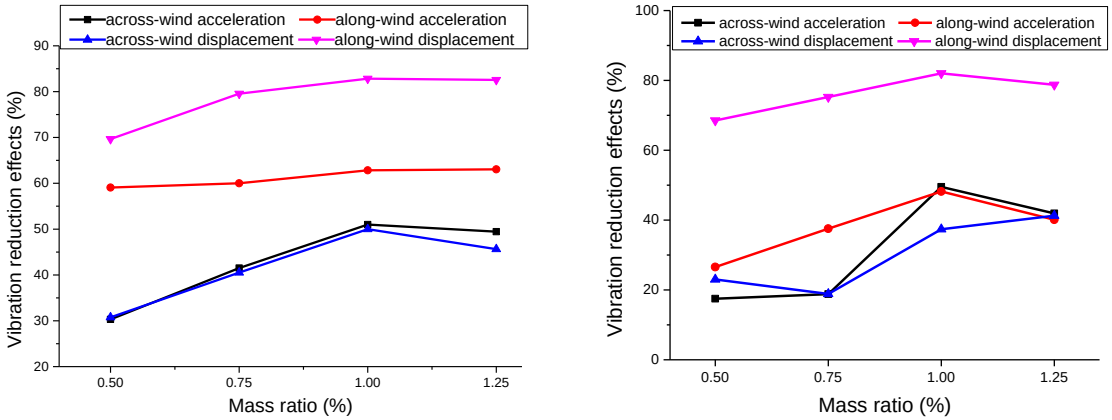

(a) RMS response (b) Peak value response

Fig. 10 Vibration reduction effects under different mass ratios

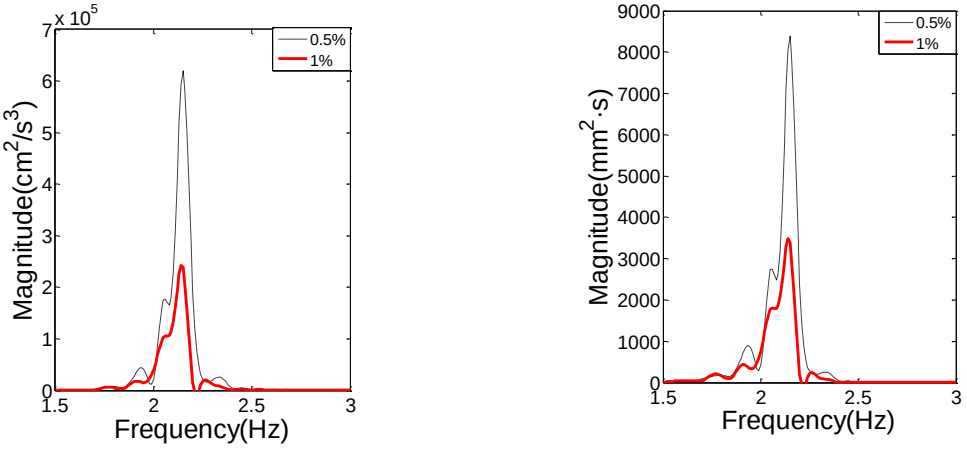

(a) Acceleration response (b) Displacement response

Fig. 11 Power spectral density under different mass ratios (0.5% and 1%)

Through the above analyses and conclusion in part 4.1, relatively larger mass ratios and lighter particle density are suggested in the design process of the PTMD (with the stipulation that the particles are not piled up in many layers). On the one hand, the peak value of the primary structure power spectrum can be effectively reduced by increasing the mass ratio; and on the other hand, the lighter particle density can make the vibration energy be distributed in a broader frequency band, thus dissipating much more vibration energy.

4.3 Effects of mass ratio of container to particles

The influence of the mass ratio of the container to particles (0.056, 0.25, 0.5, 1, 2, 4, infinite) was examined by keeping the particle material (lead), the particle diameter (2 mm), the total auxiliary mass ratio (1%), the container size (8.5 cm×8.5 cm, 2 layers) and the wind velocity (4 m/s) constant.

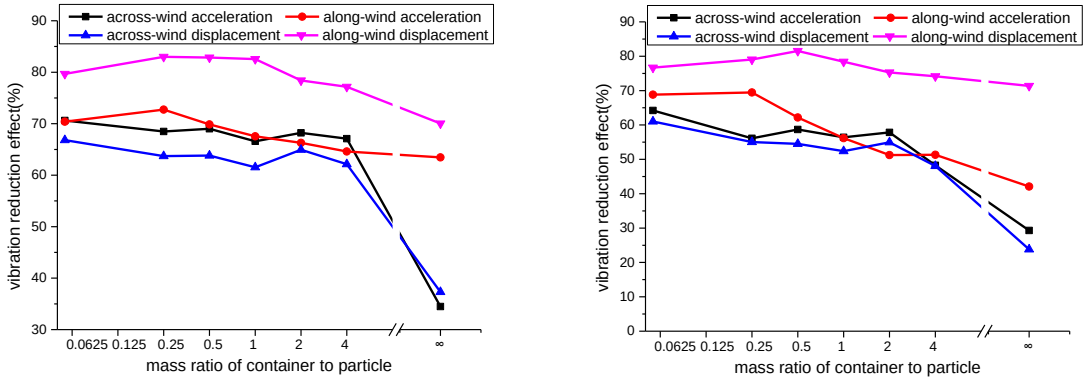

(a) RMS response (b) Peak value response

Fig. 12 Vibration reduction effect under different mass ratios of the container to particles

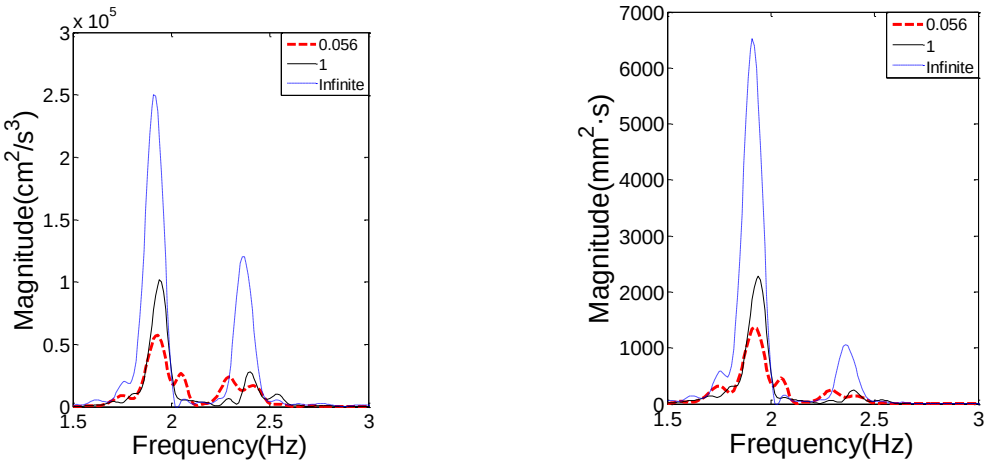

(a) RMS response (b) Peak value response

Fig. 13 Power spectral density under different mass ratios of the container to particles (0.056, 1 and infinite)

Fig. 12 shows that the vibration reduction effects decrease as the mass of particles decreases (resulting in an increase of the container mass, with the same total auxiliary mass). The reason is that the PTMD can dissipate input energy not only by tuning the frequency just like the classical TMD, but also by collisions, impact and friction between the particles and the container. The decrease of the particle mass may reduce the energy dissipation of such part. When the total mass of particles turns to zero, at which time the PTMD becomes a TMD, the reduction effects are much worse. The results also indicate that the reduction effects of PTMD are better than that of TMD under wind excitations.

Fig. 13 shows the power spectrum of the vibration response when the ratio is 0.056, 1 and infinite, respectively. The highest magnitude occurs when the ratio is infinite. The peak value of the magnitude reduces, and the frequency band becomes broader with the ratio decreasing, indicating that increasing particles can transfer more vibration energy from the primary structure to the attached damper, and at the same time distribute the vibration energy of the primary structure within a broader frequency band. The analysis suggests that increasing the particle mass can reduce the vibration response effectively when the total auxiliary mass ratio of the damper to primary structure is constant.

4.4 Effects of suspending length

The natural frequency of the building is influenced heavily by the surrounding environment (such as temperature, humidity, heavy rain and strong wind) in actual projects. The traditional TMD has favorable damping performance under specific tuning frequencies, but the vibration reduction effect is not stable when the frequency is not optimally tuned. On the other hand, the PTMD reduces the vibration energy not only through the tuned frequency, but also by impact and friction between particles and the container wall. Consequently, it is very important and meaningful to investigate the damping performance of the PTMD when the damper frequency is not consistent with the natural frequency of the primary structure.

In the experiment under discussion, different damper frequencies can be realized by adjusting the suspending length. The suspending length of 4 cm, 5 cm, 6 cm and 7 cm are separately adopted and the corresponding frequencies are 2.49 Hz, 2.29 Hz, 2.03 Hz and 1.88 Hz, respectively. The particle material (tungsten carbide), the mass ratio (1%), the particle diameter (6 mm), the container size (8.5 cm×8.5 cm, 2 layers) and the wind velocity (4 m/s) were kept constant. The damping performance is shown in Table 4, and the damping law under different tuning frequencies is highly consistent with the experiment and simulation results conducted by Saeki (2002). The most favorable reduction effect happens in the case of 6 cm (61%-86%), and the reason is that the attached damper increases the total mass and then lowers the natural frequency of the primary structure. More importantly, the reduction effects under the other suspending lengths are also favorable, indicating the robustness of the PTMD. The damping effects for all the cases are ranging from 41% to 86%.

The peak value of the uncontrolled structure is much higher than that of the controlled one, so the power spectrum does not include that peak value (the curve is clipped for added resolution). From the comparison of the power spectrum in Fig. 14, the peak value in the case of 6cm is the lowest and the broadest frequency band happens in the case of 5cm and 6cm. The frequency band becomes broader with the diminishing span between the suspending length and tuning length. The above analysis shows that the PTMD has satisfactory damping performance, even when the frequency is not tuned, and also emphasizes the robust damping performance of the PTMD and its

effective application prospects in civil engineering.

4.5 Wind velocity

In practical projects, the applied wind load under extreme events is inevitably larger than the design load specified in the load code, so the most unfavorable situation should be considered in the design process of the particle tuned damper. In this section, five different wind velocities were considered: 3 m/s, 3.5 m/s, 4 m/s, 4.5 m/s, 5 m/s, and the specified wind velocity is 4 m/s. The total mass ratio (1%), the particle material (steel), the particle diameter (6 mm), and the container size (7 cm×7 cm, 2 layers), were kept constant.

The results are shown in Fig. 15. The vibration reduction effects become better with increasing wind velocity, but the relationship between them is non-linear. As the excitation level increases, the efficiency of the damper increases too, due to the fact that the more energetic motion of the particles increases the exchange of momentum. On the other hand, when the excitation is high enough to mobilize all the particles, the response amplitude becomes independent of the intensity of the excitation (Lu *et al*. 2011). The results show that the damping performance of the PTMD under stronger (than design) wind is generally superior to that under the specified (design) wind excitation.

Table 4 The RMS damping effects under different suspending lengths

Suspending length	4cm (2.49Hz)	5cm (2.29Hz)	6cm (2.03Hz)	7cm (1.88Hz)
Across-wind acceleration	44.00%	50.72%	67.72%	61.73%
Along-wind acceleration	45.03%	54.08%	60.90%	60.19%
Across-wind displacement	40.89%	48.17%	65.97%	64.70%
Along-wind displacement	77.49%	83.76%	86.06%	76.30%

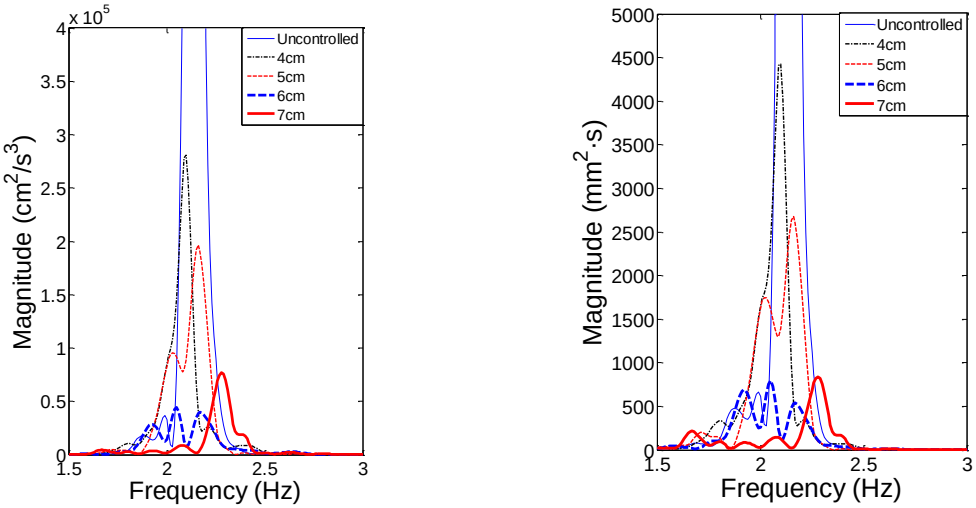

(a) Acceleration response (b) Displacement response

Fig. 14 Power spectral density under different suspending lengths

5. Experiment simulation

5.1 PTMD simulation

The results of the experiments discussed above can be used to optimally design a PTMD for a structure that is excited by wind pressure. The precise analysis of a dynamic system with an attached PTMD is quite complex for the random of wind excitations and multi-directions movements of the primary structure. Consequently, the developed single-particle damper theory is used to generalize the results. This is accomplished by replacing the particles in the PTMD with a single particle having the equivalent mass, coefficient of restitution, and clearance (Papalou and Masri 1996).

The principles of equivalence are as follows:

- The density and total mass of particles are kept constant.
- The empty volume in a single-particle damper is equal to that in the PTMD.

The shape of the simplified container is a cylinder, and its bottom diameter is equal to the diameter of the simplified single particle (D).

The simplification diagram is shown in Fig. 16, based on the above principles.

5.2 Structure simulation

The diagram of main structure with simplified PTMD is shown in Fig. 17(a). Considering the symmetry and evenly mass distribution, the primary structure (as it shown in Fig. 1(b)) can be modeled as an n DOFs vertical linear cantilever beam, then the suspended container of PTMD will be the (n+1)*th* DOF, which mass, damping and stiffness are denoted by m_c, c_c and k_c, respectively. The impact force produced by the impact between the simplified particle and its container walls can be treated as an external force (w_p) which is applied to the (n+1)*th* DOF (the container), the simplified model is shown in Fig.17(b).

According to the above analysis, the equation of motion of the primary system with the attached PTMD can be written as Eq. (2)

$$\begin{aligned} \mathbf{M}\ddot{x} + \mathbf{C}\dot{x} + \mathbf{K}x &= \mathbf{W}(t) + \varphi(c_c\dot{z}_1 + k_c z_1) \\ m_c\ddot{x}_c + c_c\dot{z}_1 + k_e z_1 - c_p H(z_2,\dot{z}_2) - k_p G(z_2) &= 0 \\ m_p\ddot{x}_p + c_p H(z_2,\dot{z}_2) + k_p G(z_2) &= 0 \end{aligned} \tag{2}$$

$$\mathbf{M} = \mathrm{diag}[m_1 \quad m_2 \quad \ldots \quad m_n] \tag{3}$$

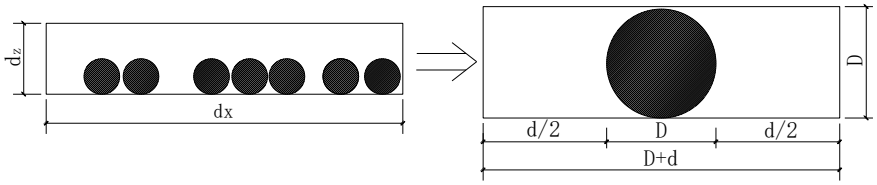

Fig. 16 Diagrams of particle damper and simplified single particle damper

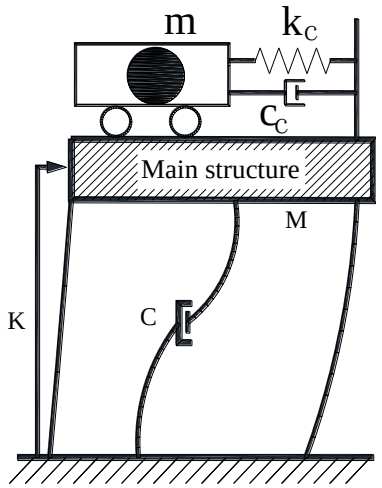

(a) Primary structure with simplifed PTMD

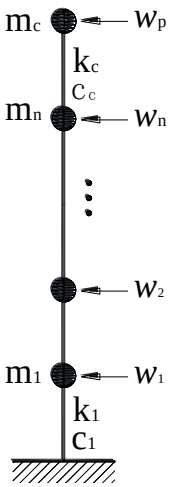

(b) Simplified diagram of main strucuture under wind load

Fig. 17 Simplified diagrams of the test model with PTMD

$$\mathbf{C}=\begin{bmatrix} c_1+c_2 & -c_2 & & & \\ -c_2 & c_2+c_3 & -c_3 & & \\ & -c_3 & \ldots & & \\ & & & \ldots & -c_n \\ & & & -c_n & c_n \end{bmatrix} \tag{4}$$

$$\mathbf{K}=\begin{bmatrix} k_1+k_2 & -k_2 & & & \\ -k_2 & k_2+k_3 & -k_3 & & \\ & -k_3 & \ldots & & \\ & & & \ldots & -k_n \\ & & & -k_n & k_n \end{bmatrix} \tag{5}$$

$$\mathbf{W}(t)=[w_1(t) \quad w_2(t) \quad \ldots \quad w_n(t)]^T \tag{6}$$

$$\varphi=[0 \;\; 0 \ldots 0 \;\; 1]^T \tag{7}$$

$$z_1 = x_n - x_c \tag{8}$$

$$z_2 = x_c - x_p \tag{9}$$

Where **M**, **C** and **K** are the mass, damping, and stiffness matrixes of the primary structure, respectively; x is an N-dimensional displacement vector of the structure; **W**(t) is an N-dimensional wind excitation vector; φ is an N-dimensional location vector of control force, whose nth

component is 1 and the other components are 0; x_c is the displacement of the container, and x_p is the displacement of the simplified particle; z_1 is the relative displacement of the container with respect to the primary system, and z_2 is the relative displacement of the simplified particle with respect to the container.

Furthermore, the following parameters characterize the container: $k_c=m_c\omega_c^2$, $c_c=2m_c\zeta_c\omega_c$, $\omega_c=2\pi f_c$, $f_c=1/(2\pi)(g/l)^{0.5}$, l is the suspending length from the top of the model to the center of the container.

Similarly, the following parameters characterize the equivalent damper particle: $k_p=m_p\omega_p^2$, $c_p=2m_p\zeta_p\omega_p$, ζ_p is the fraction of critical damping of the impact damper "stops", ω_p is the natural frequency of the impact damper "stops".

The functions $G(z_2)$ are nonlinear functions shown in Fig. 18, and the expression of $H(z_2,\dot{z}_2)$ is shown in Eq. (10), representing the nonlinear characteristics of the damper. By a proper choice of ω_p, the nonlinear springs $G(z_2)$ can simulate a rigid barrier to any degree of accuracy, based on previous studies. The parameter ζ_p in conjunction with $H(z_2,\dot{z}_2)$ provides means for simulating inelastic impacts, ranging from the completely plastic up to the elastic ones, so the value of any desired coefficient of restitution e can be adjusted by setting the appropriate value for ζ_p according to Masri and Ibrahim (1972, 1973).

$$H(z_2,\dot{z}_2)=\begin{cases}0; & -d/2<z_2<d/2\\ \dot{z}_2; & z_2\geq d/2 \ or \ z_2\leq -d/2\end{cases} \tag{10}$$

5.3 wind load simulation

In the wind tunnel experiment, the primary structure undergoes both along-wind and across-wind motions under wind excitations, so that the PTMD vibrates in both directions. For simplicity, a simplified single particle damper in each direction will be considered. The main justification for making the above simplifications is that our main propose is to primarily evaluate the damper performance of PTMD under wind excitation, and give further reference to the more sophisticated research, which will involve more computational efforts, will be considered after more experience is gained through the present study (Yang *et al.* 2004).

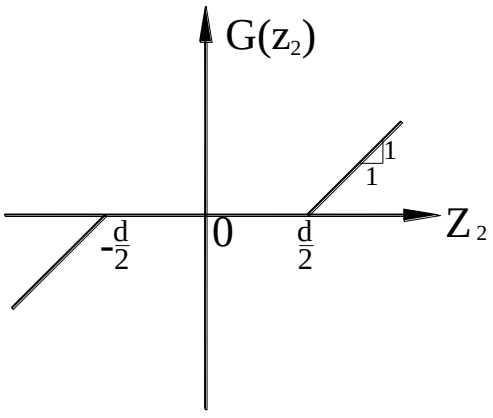

Fig. 18 Nonliear function of particle damper

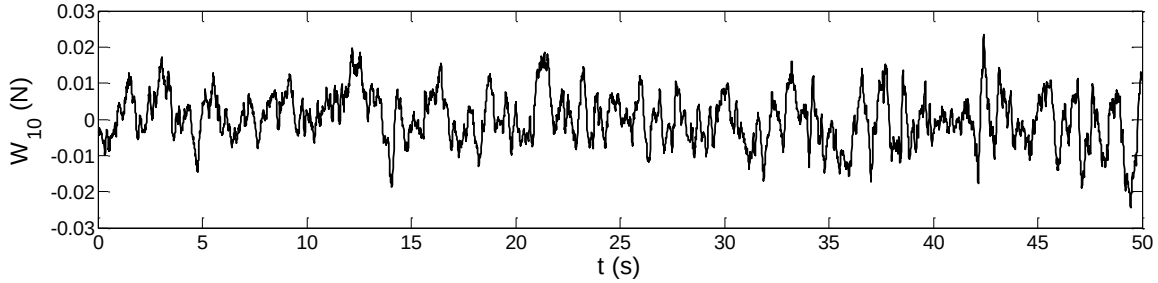

Fig. 19 The across-wind load time histories on 10th floor location

In this study, the across-wind vibration is simulated because of its controlling nature in the total structure vibration. The mass and the stiffness of the model are distributed evenly along the height, so the 10DOFs system is adopted to simulate the whole primary structure.

The across-wind load is mainly caused by the vortex shedding which is vertical to the wind flow. The complex mechanism and building shape dependence make it hard to simulate precisely. The wind tunnel pressure tests of the benchmark model used in the experiment were conducted at the University of Sydney. Detailed descriptions of the wind tunnel tests to generate across-wind data are given in Samali *et al.* (2004), and the time histories of across-wind load are all available at the website (SSTL 2002). In this article, the wind tunnel data can be calculated based on the theory in Samali *et al.* (2004) and similarity principles of wind tunnel tests. One example of the obtained across-wind load pressure time history on the 10th story is shown in Fig. 19.

5.4 Parameter determination

The parameters are determined according to the pervious test and includes three parts: the main structure, the container and the particles.

1). Main structure

As it is shown in section 2.3, the total mass of the model is 19.2 kg, and Table 3 shows that the test model frequency and damping ratio is 2.17 Hz and 0.003, respectively. Therefore, the corresponding circular frequency is 13.63 rad/s.

2). Container

The test mass of the container is 0.01 kg, and the test circular frequency is 13.63 rad/s, which is same to the main structure. As the damping ratio of the wooden container is difficult to test in the experiment, the determination of such parameter is obtained by trial-and-error calculations. Fig. 20 shows the vibration response on the top of primary structure under different container damping ratios. It is shown that the vibration response does not change much when the damping ratio of the container is lower than 0.05. This phenomenon indicates that the damping ratio of the container is not sensitive to the final response as long as the value being less than 0.05. Considering the container is connected by four soft round lines and it can swing freely at the top space of the model, the damping ratio is finally assumed to be 0.005.

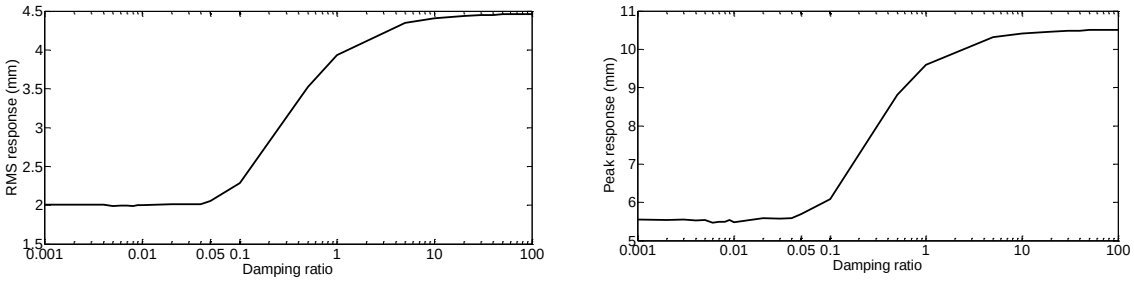

(a) RMS of displacement response (b) Peak displacement response

Fig. 20 The vibration response at the top of primary structure under different container damping ratios

3). Particles

The particles are 6mm diameter steel balls. Because the mass ratio of PTMD to main structure is 1%, the total mass of container and particles is 0.192 kg, then the particles' mass is 0.182 kg. The steel particle test density is 7644 kg/m^3 and the container size is 8.5 cm×8.5 cm, with two layers. Consequently, the calculated total number of the particles is 209 and corresponding filling ratio is 27.5%. The Eq. (11) shows the calculated equation of filling ratio.

$$\rho_p = \frac{V_{particles}}{V_{container}} = \frac{0.182/7644}{0.085\times 0.085\times 0.006\times 2} = 27.5\% \tag{11}$$

The coefficient of restitution e of steel is 0.5, the equivalent circular frequency and the critical damping ratio of particles are based on the previous research of Masri (1973).

According to the above analysis, the parameters used in the numerical simulation are listed in Table 5.

Table 5 Values of system parameters

	Parameter	Value
Main structure	Total mass (kg)	19.2
	Circular frequency (rad/s)	13.63
	Damping ratio	0.003
Container	Mass (kg)	0.01
	Circular frequency (rad/s)	13.63
	Damping ratio	0.005
Particles	Total mass (kg)	0.182
	Equivalent circular frequency (rad/s)	13.63
	Coefficient of restitution	0.5
	Critical damping ratio	0.2
	Filling ratio (%)	27.5
	Material density (kg/m^3)	7644
	Diameter (mm)	6

5.5 Simulation results

Using the established dynamic model, a numerical simulation was carried out by employing the fourth-order Runge-Kutta method. The comparative results between the test and the simulation of primary structure are shown in Table 6, in which, σ_x and $\sigma_{\ddot{x}}$ represent the RMS values of the 10th floor displacement x and acceleration $\ddot{x}$, respectively, and x_{max} and $\ddot{x}_{max}$ represent the peak value of the 10th floor displacement x and acceleration $\ddot{x}$, respectively.

It can be seen from Table 6 that there is a good agreement between the simulation and experimental results when the primary structure is under no control condition. This demonstrates that the simulation of the wind load and model dynamic characteristic is appropriate, and also, this accuracy is the keystone of the next procedure of the simulation of the primary system with PTMD. The following reasonable agreement of the test and experimental results after attaching PTMD is also shown in Table 6. It demonstrates that the proposed analytical method can yield estimates of the response of the controlled structure under wind conditions with an acceptable accuracy.

Figs. 21 and 22 show sample 10 seconds high-resolution plots of the simulation results, with a comparison of the response of the primary structure with and without the PTMD. It can be seen that the PTMD has favorable damping performance under wind excitation; the time history curves show similar characters which is depicted in the experiment discussed in Section 4.1, and the high frequency components of the impact damper case is also clearly shown in Fig. 22.

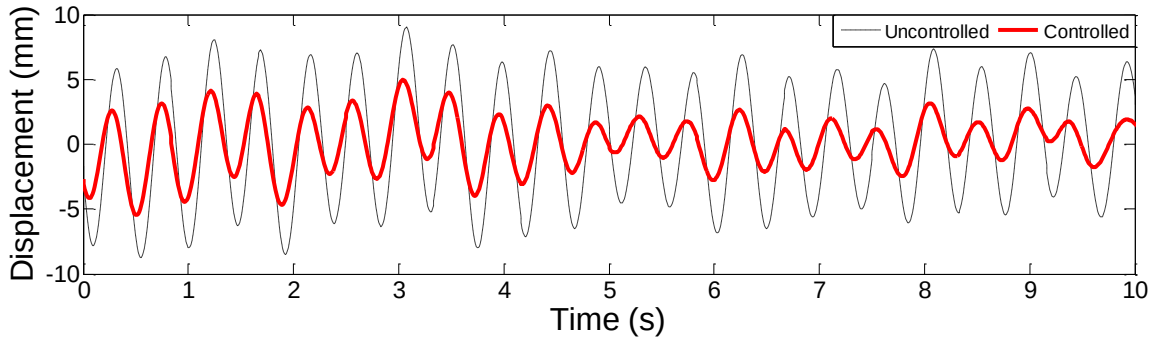

Fig. 21 The simulation result for displacement response at the top of the model

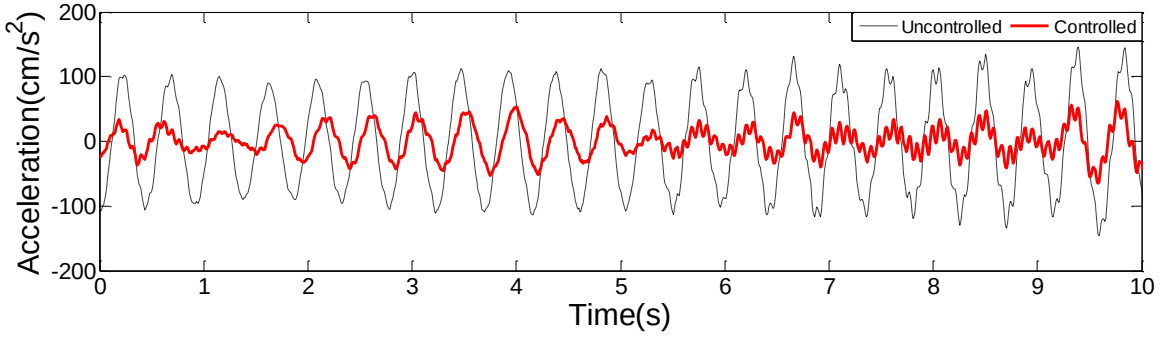

Fig. 22 The simulation result for accleration response at the top of the model

Table 6 Comparison of test and simulation results

	σ_x (mm)			$\sigma_{\ddot{x}}$ (cm/s^2)		
	Test	Simulation	Error (%)	Test	Simulation	Error (%)
Uncontrolled	4.05	4.16	2.66	77.73	76.31	-1.82
Controlled	2.00	2.00	0.00	37.64	37.90	0.70
	x_{max} (mm)			$\ddot{x}_{max}$ (cm/s^2)		
	Test	Simulation	Error (%)	Test	Simulation	Error (%)
Uncontrolled	11.02	11.61	5.40	203.51	204.83	0.65
Controlled	5.56	5.55	-0.27	127.61	123.32	-3.36

From the simulation results, it can be concluded that the approximate simulation method with reasonable parameter determinations can yield an acceptable estimation of the response of the primary structure with an attached PTMD control device. Both the calculated RMS value and the peak value of the displacement and the acceleration under wind excitations agree with experimental results with fairly good accuracy.

5. Conclusions

A particle tuned mass damper system was proposed, and a detailed aero-elastic wind tunnel experiment was conducted in order to investigate the damping performance of the proposed damper configuration. The influence of some key system parameters (such as particle density, total auxiliary mass ratio, mass ratio of the container to particles, suspending length, and wind velocity) on the behavior of the PTMD was discussed. Furthermore, theoretical analyses, based on the measured wind excitation and equivalent simplified single particle principles, were conducted to simulate the experimental results.

It is found that significant improvements in damping effectiveness are achieved with respect to the reduction of particle density and mass ratio of the container to particles. Also, higher values of mass ratio and strong wind excitations generally result in a proportionally non-linear improvement of the damping performance. Furthermore, the robustness of the PTMD is verified under different tuning frequencies. By generalizing the experimental results, some guidelines are given for the optimum design of the PTMD, in conjunction with a lightly damped high-rise building, to achieve a relatively large reduction in the primary structure's response while incorporating a small weight penalty. The theoretical analysis results show favorable agreement with the experimental results, and further prove the effectiveness of the damping performance of the particle tuned mass damper system under broad-band wind excitation. It is expected that the application prospect of the particle tuned mass damper is quite promising in the wind-induced vibration control area of high-rise buildings.

Acknowledgments

Financial support from the National Natural Science Foundation of China through grant 51478361 and the Fundamental Research Funds for the Central Government Supported Universities are highly appreciated.

References

Aly, A.M. (2013), "Vibration control of high-rise buildings for wind: a robust passive and active tuned mass damper", *Smart Struct. Syst*., **13**(3), 473-500.

ASCE Manual of Practice No. 67 on Wind Tunnel Studies of Buildings and Other Structures, ASCE.(2003).

Andreaus, U., Baragatti, P. and Placidi, L. (2016), "Experimental and numerical investigations of the responses of a cantilever beam possibly contacting a deformable and dissipative obstacle under harmonic excitation" , *Int. J. Nonlinear Mech.*, **80**(1), 96-106.

Andreaus, U., Chiaia, B. and Placidi, L. (2013a), "Soft-impact dynamics of deformable bodies", *Continuum Mech. Therm*., **25**(2), 375-398.

Andreaus, U., Placidi, L. and Rega, G. (2010), "Numerical simulation of the soft contact dynamics of an impacting bilinear oscillator", *Commun. Nonlinear Sci, Numer, Simul*.,**15**(9), 2603-2616.

Andreaus, U., Placidi, L. and Rega, G. (2013b), "Microcantilever dynamics in tapping mode atomic force microscopy via higher eigenmodes analysis", *J. Appl. Phys.*, **113**(22), 224302.

Bryce, L.F., Eric, M.F. and Steven, E.O. (2000), "Effectiveness and predictability of particle damping", *Proceedings of the SPIE's 7th Annual International Symposium on Smart Structures and Materials*, International Society for Optics and Photonics

Campbell, R. (1995). "A true tall tale about the Hancock Tower", *Boston Globe*. **3**.

Clinton, J.F., Bradford, S.C., Heaton, T.H. and Favela, J. (2006), "The observed wander of the natural frequencies in a structure", *Bull. Seismol. Soc. Am*., **96**(1), 237-257.

Chiaia, B., Kumpyak, O., Placidi, L. and Maksimov, V. (2015), "Experimental analysis and modeling of two-way reinforced concrete slabs over different kinds of yielding supports under short-term dynamic loading", *Eng. Struct.*. **96**, 88-99.

Dell'Isola, F., Della Corte, A., Greco, L. and Luongo, A. (2015). "Plane bias extension test for a continuum with two inextensible families of fibers: A variational treatment with Lagrange multipliers and a perturbation solution", *Int. J. Solids Struct.*, **81**, 1-12.

Esteki, K., Bagchi, A. and Sedaghti, R. (2015), "Semi-active control of seismic response of a building using MR fluid-based tuned mass damper", *Smart Struct. Syst.*, **16**(5), 807-833.

Ghorbani−Tanha, A.K., Noorzad, A. and Rahimian, M. (2009), "Mitigation of wind-induced motion of Milad Tower by tuned mass damper", *Struct. Des. Tall Spec. Build*., **18**(4), 371-385.

Gu, M. and Peng, F. (2002), "An experimental study of active control of wind-induced vibration of super-tall buildings", *J. Wind Eng. Ind. Aerod*., **90**(12), 1919-1931.

Gu, M. and Quan, Y. (2004), "Across-wind loads of typical tall buildings", *J. Wind Eng. Ind. Aerod*., **92**(13), 1147-1165.

Housner, G.W., Bergman, L.A., Caughey, T.K., Chassiakos, A.G., Claus, R.O., Masri, S.F., Skelton, R.E., Soong, T.T., Spencer, B.F. and Yao, J.T.P. (1997), "Structural control: past, present, and future", *J. Eng. Mech. – ASCE*, **123**(9), 897-971.

Hu, L., Huang, Q.B. and Liu, Z.X. (2008), "A non-obstructive particle damping model of DEM", *Int. J. Mech. Mater. Des*., **4**(1), 45-51.

Karamodin, A. and Haji Kazemi, H. (2015), "Nonlinear control of structure using neuro-predictive algorithm", *Smart Struct. Syst*., **16**(6), 1133-1145.

Lu, X. and Chen, J. (2011a), "Mitigation of wind−induced response of Shanghai Center Tower by tuned mass damper", *Struct. Des. Tall Spec. Build*., **20**(4), 435-452.

Lu, X. and Chen, J. (2011b), "Parameter optimization and structural design of tuned mass damper for shanghai centre tower", *Struct. Des. Tall Spec. Build*., **20**(4), 453-471.

Lu, Z., Lu, X.L., Lu, W.S. and Masri, S.F. (2012), "Shaking table test of the effects of multi-unit particle dampers attached to an MDOF system under earthquake excitation", *Earthq. Eng. Struct. D*., **41**(5), 987-1000.

Lu, Z., Lu, X.L. and Masri, S.F. (2010), "Studies of the performance of particle dampers under dynamic loads", *J. Sound Vib*., **329**(26), 5415-5433.

Lu, Z., Masri, S.F. and Lu, X.L. (2011a), "Parametric studies of the performance of particle dampers under harmonic excitation", *Sturct. Control Health Monit.*, **18**(1), 79-98.
Lu, Z., Masri, S.F. and Lu, X.L. (2011b), "Studies of the performance of particle dampers attached to a two-degree-of-freedom system under random excitation", *J. Vib. Control*, **17**(10), 1454-1471.
Lu, Z., Wang, D.C. and Li, P.Z. (2014), "Comparison study of vibration control effects between suspended tuned mass damper and particle damper", *J. Shock Vib.*. **2014**.
Masri, S.F. and Ibrahim, A.M. (1973), "Response of the impact damper to stationary random excitation", *J. Acoust. Soc. Am*., **53**(1), 200-211.
Masri, S.F. and Ibrahim, A.M. (1972), "Stochastic excitation of a simple system with impact damper", *Earthq. Eng. Struct. D.*, **1**(4), 337-346.
Naeim, F., Lew, M. and Carpenter, L.D. (2011), "Performance of tall buildings in Santiago, Chile during the 27 February 2010 offshore Maule, Chile earthquake", *Struct. Des. Tall Spec. Build*., **20**(1), 1-16.
Papalou, A. and Masri, S.F. (1996), "Performance of particle dampers under random excitation", *J. Vib. Acoust. – T- Asme.* **118**(4), 614-621.
Papalou, A. and Strepelias, E. (2014), "Effectiveness of particle dampers in reducing monuments' response under dynamic loads", *Mech. Adv. Mater. Struct*., **23**(2),128-135.
Petersen, N.R. (1980), "Design of large scale tuned mass dampers", *Struct. Control*, 581-596.
Piccardo, G., Tubino, F. and Luongo, A. (2015), "Equivalent nonlinear beam model for the 3-D analysis of shear-type buildings: Application to aeroelastic instability", *Int. J. Nonlinear Mech*., **80**, 52-65.
Quan, Y. (2002), "Super high-rise building's wind loads and response in across-wind direction", Ph.D. Dissertation, Tongji University, Shanghai.
Saeki, M. (2002), "Impact damping with granular materials in a horizontally vibrating system", *J. Sound Vib*., **251**(1), 153-161.
Samali, B., Kwok, K., Wood, G. and Yang, J. N. (2004), "Wind tunnel tests for wind-excited benchmark building", *J. Eng. Mech. – ASCE*, **130**(4), 447-450.
Sharma, S., Vig, R. and Kumar, N. (2015), "Active vibration control: considering effect of electric field on coefficients of PZT patches", *Smart Struct. Syst*., **16**(6), 1091-1105.
Sims, N.D., Amarasinghe, A. and Ridgway, K. (2005), "Particle dampers for workpiece chatter mitigation", *Manuf. Eng.*, **16**(1), 825-832.
Smart Structures Technology Laboratory (SSTL). (2002), "Structural control: Benchmark comparisons", <http://www.nd.edu/~quake/bench.html>
Tanaka, H. and Mak, C. (1983), "Effect of tuned mass dampers on wind induced response of tall buildings", *J. Wind Eng. Ind. Aerod*., **14**, 357-368.
Vickery, B.J., Davenport, A.G. and Wargon, C. (1970), An Investigation Of The Behaviour In Wind Of The Proposed Centrepoint Tower In Sydney, Australia, Boundary Layer Wind Tunnel Laboratory, Faculty of Engineering Sciences, University of Western Ontario, London, Ontario, Canada.
Warnitchai, P. and Hoang, N. (2006), "Optimal placement and tuning of multiple tuned mass dampers for suppressing multi-mode structural response", *Smart Struct. Syst.*, **2**(1), 1-24.
Yan, W., Xu, W.B., Wang, J. and Chen, Y.J. (2013), "Experimental research on the effects of a tuned particle damper on a viaduct system under seismic loads", *J. Bridge Eng*., **19**(3).
Yang, J.N., Agrawal, A.K., Samali, B. and Wu, J.C. (2004), "Benchmark problem for response control of wind-excited tall buildings", *J. Eng. Mech.- ASCE*, **130**(4), 437-446.
Yao, J.T.P. (1972), "Concept of structural control", *J. Struct. Div. – ASCE*, **98**(7), 1567-1574.